Heliyon 10 (2024) e34689

Contents lists available at ScienceDirect

Heliyon

journal homepage: www.cell.com/heliyon

Research article

Highly efficient electrocatalytic oxidation of levodopa as a Parkinson therapeutic drug based on modified screen-printed electrode

Tan Wang [a], Nadhir N.A. Jafar [b], Afrah Majeed Ahmed Al-Rihaymee [c], Dheyaa Yahaia Alhameedi [d], Fadhil A. Rasen [e], Furqan S. Hashim [f], Talib Kh Hussein [g], Montather F. Ramadan [h], Kasim Kadhim Alasedi [i], Muath Suliman [j,*], Ahmed Hussien Alawadi [k,l,m]

[a] Three Gorges University, College of Basie Medical Scienees, 443002, China
[b] Al-Zahraa Center for Medical and Pharmaceutical Research Sciences (ZCMRS), Al-Zahraa University for Women, Karbala, 56001, Iraq
[c] Anesthesia Techniques Department, College of Health and Medical Techniques, Al-Mustaqbal University, 51001, Babylon, Iraq
[d] Department of Anesthesia, College of health & medical Technology, Sawa University, Almuthana, Iraq
[e] Department of Medical Engineering, Al-Esraa University College, Baghdad, Iraq
[f] Department of Medical Laboratories Technology, AL-Nisour University College, Baghdad, Iraq
[g] Al-Hadi University College, Baghdad, 10011, Iraq
[h] College of Dentistry, Al-Ayen University, Thi-Qar, Iraq
[i] Department of Medical Laboratory Techniques, Altoosi University College, Najaf, Iraq
[j] Department of Clinical Laboratory Sciences, College of Applied Medical Sciences, King Khalid University, Abha, Saudi Arabia
[k] College of technical engineering, the Islamic University, Najaf, Iraq
[l] College of technical engineering, the Islamic University of Al Diwaniyah, Iraq
[m] College of technical engineering, the Islamic University of Babylon, Iraq

ARTICLE INFO

Keywords:
Levodopa
Zinc oxide
Cobalt oxide
Nanocomposite
Screen-printed electrode

ABSTRACT

The current study presents the creation of a straightforward and sensitive sensor based on ZnO/Co_3O_4 nanocomposite modified screen-printed electrode (ZnO/Co_3O_4NC/SPE) for levodopa determination. At ZnO/Co_3O_4NC/SPE, an oxidative peak for levodopa solution in pH 6.0 phosphate buffer solution (PBS) were seen that were both more resolved and more enhanced. Levodopa was measured using differential pulse voltammetry (DPV), which showed an excellent linear range (0.001–800.0 μM) and detection limit (0.81 nM). The presence of interference did not affect the electrochemical response of levodopa at ZnO/Co_3O_4NC/SPE, demonstrating high selectivity. Levodopa in a real samples have been successfully detected using the manufactured sensor.

1. Introduction

Since the 1960s, levodopa (l-3,4-dihydroxyphenylalanine), a direct precursor of dopamine, has been the most effective symptomatic medicine for the treatment of Parkinson's disease (PD) [1,2]. Lack of dopamine, which cannot be carried directly into the brain because of the blood-brain barrier, is a crucial factor in Parkinson's disease [3]. Levodopa, which may be converted into dopamine in

* Corresponding author.
E-mail address: dr.muathsuliman@gmail.com (M. Suliman).

https://doi.org/10.1016/j.heliyon.2024.e34689
Received 30 January 2024; Received in revised form 14 July 2024; Accepted 15 July 2024
Available online 21 July 2024

the brain under the influence of dopamine decarboxylase, is frequently required as an alternate therapy for sufferers [4].

Levodopa can successfully treat a variety of Parkinson's disease symptoms, but the dose issue continues to perplex medical professionals [5]. The condition cannot be successfully stopped by underdosing, while overdose might have a variety of negative side effects, such as dyspraxia, myospasm, mental disorders, etc. Additionally, the challenges of therapeutic dosage regulation are exacerbated by individual variations in drug impact and drug metabolism [6–8]. Levodopa in human serum must thus be found throughout PD therapy to regulate medication safety along with patient health. Levodopa monitoring techniques are gas chromatography (GC), capillary electrophoresis, high performance liquid chromatography (HPLC), flow injection analysis and photokinetic methods, among others [9–13]. However, each method has drawbacks, including selectivity, price, lengthier analytical times and the use of organic solvents, as well as sample preparation [14–17]. Indeed, several studies on the electroanalytical determination of analytes by voltammetric techniques have been published with great operating conditions, such as simplicity, speed, sensitivity, precision, and affordability [18–22]. As a result, it appears that there is a need for point-of-care and on-site analysis, as well as a switch from popular old procedures to new, potent methods [23–26]. The analyte oxidation at the surface of frequently used bare electrodes, in contrast, is hampered by a large overpotential, thus it is a good idea to change the surface of electrodes with the proper materials [27–30].

ZnO is a (n)-type semiconductor with unique properties that make it useful in many different kinds of devices, such as chemical gas sensors, laser diodes, biosensors, ultraviolet photodetectors, and transparent conductive oxide [31–37]. Nanomaterials may be employed as the best sensing materials since they have a very high surface to volume ratio along with a very big surface area [38–41].

But despite all the advantages, there are still certain issues that need to be resolved. The need for sensors with cutting-edge capabilities in low concentration analytes has grown in recent years [42,43]. Other extra strategies must be included in order to increase the sensing capabilities due to the fact that it is challenging to manufacture sensors with more enhanced selectivity and response using just bare ZnO nanoparticles. Techniques including ion implantation, core/shell structure construction, decorating with noble metal or metal oxide nanoparticles, and structural modification have improved the sensing capabilities [44–49]. In order to enhance the sensing capabilities, in this work, ZnO nanoparticles were coated with Co_3O_4 nanoparticles, (p)-type semiconductors. Synergistic interactions between these two nanomaterials may improve the analyte sensing characteristics since Co_3O_4 is a very sensitive material [50]. Additionally, the ranges of possible energy barriers among (n)-ZnO and (p)-Co_3O_4 are expected to change, increasing the resistance of the sensors to analyte exposure and enhancing responsiveness [51].

In this work, for the first time a spherical morphology of nanocomposite consisting of ZnO/Co_3O_4 nanocomposite (ZnO/Co_3O_4 NC) was synthesized by an ultrasound assisted method. The result illustrates that the particles' shape is amorphous when ultrasonic irradiation is absent and the particle size has been bigger than the nanoscale size. According to the above points, we used this important kind of composite for the modification of the screen-printed electrode (SPE). Meanwhile, the surface detection properties have been analyzed by evaluating their cyclic voltammetry (CV). Then, voltammetry techniques were used to investigate the electrochemical properties of levodopa oxidation at the modified electrode. Levodopa's anodic peak current may be dramatically raised and its oxidation can be much improved due to the attractive properties of ZnO/Co_3O_4 NC/SPE. Additionally, research has been done on the modified electrode's repeatability and stability for levodopa detection. Ultimately, the suggested technique was applied to ascertain the levodopa content of actual samples.

2. Experimental

2.1. Materials

Polyvinylpyrrolidone (PVP), sodium hydroxide, zinc nitrate hexahydrate ($Zn(NO_3)_2{\cdot}6H_2O$), cobalt nitrate hexahydrate ($Co(NO_3)_2{\cdot}6H_2O$), and levodopa were among the substances purchased from Merck for this investigation. These reagents were used without any further purification in their original forms. To guarantee high cleanliness, water that had undergone double distillation was used to produce solutions.

2.2. Instrument of the study

The microstructures and morphologies of the nanocomposite created in this work were examined using a range of methods. Using an energy dispersive X-ray spectroscopy (EDS)-equipped scanning electron microscope (SEM, Hitachi SU8010) working at 15 kV, the characteristics of the nanoparticles were investigated. Glancing angled X-ray diffraction (XRD, Philips X'pert MRD pro) using Cu Kα radiation ($\lambda = 1.5418$ Å) across a 2θ range of 2°–80° was used to analyze the crystal structures. The Metrohm 710 pH meter was used to measure the pH. The Shimadzu Prominence ultrafast liquid chromatography system was used in conjunction with an AB Sciex 4000 Turbo Ion Spray tandem mass spectrometric system for liquid chromatography.

2.3. Electrochemical method

The CHI1030C Electrochemical Workstation was utilized to perform electrochemical cyclic voltammetry (CV), differential pulse voltammetry (DPV), and chronoamperometry (CHA) in the electroanalytical investigations. The usual three-electrode cell was used for these studies, and the temperature was kept constant at 25 ± 1 °C. The ZnO/Co_3O_4 NC/SPE was the working electrode, platinum wire served as the auxiliary electrode, and a saturated calomel electrode (SCE) served as the reference electrode. These three electrodes were utilized. Utilizing the CV approach, the electrochemical characteristics of the electrode were described in a potential range of −0.01 to 0.6 V in a 0.5 mM $[Fe(CN)_6]^{3-/4-}$ solution with 0.1 M KCl serving as the supporting electrolyte. DPV was used to evaluate

levodopa's electrochemical behavior and quantitative analysis throughout a voltage range of 0.02–0.75 V. After five repetitions, the results were reported in order to guarantee precision and repeatability.

2.4. Preparing ZnO/Co_3O_4 nanocomposite

Sonochemical preparation was used to create the ZnO/Co_3O_4 nanocomposite. In a conventional experiment, 1.5 M of NaOH has been dissolved in distilled water while being stirred. Drop by drop, the solution was added to a 20 mL aqueous solution containing zinc nitrate, PVP and cobalt nitrate in a 1:1:2 M ratio while being exposed to ultrasonic waves with varying irradiation powers (0, 200 and 400 W). The solution's pH was adjusted at 10. Also, the precipitate underwent a thorough deionized water wash before being baked at 100 °C. A 5-h calcination process at 650 °C has been used to create the powder.

2.5. Modification of electrode

By applying potentials between 0.4 V and 1.4 V for 15 cycles at a scan rate of 100 mV s^{-1}, the SPE was pre-treated with 0.1 M NaOH in the CV technique. The goal of this pre-treatment was to increase the electrode surface's hydrophilicity for ensuing studies. After that, a drop-coating method was used to deposit a ZnO/Co_3O_4 nanocomposite onto the SPE sensor. The nanocomposite solution was made by dissolving 1.0 mg of the nanocomposite in 1 mL of double-distilled water and ultrasonically dispersing the mixture for 60 min. Next, a carefully pipetted 5.0 μL of the composite solution was applied to the SPE surface that had been prepared. The ZnO/Co_3O_4 nanocomposite-modified SPE sensor was prepared for the electrochemical evaluation of levodopa after it had dried.

2.6. Real sample

The urine samples that have been taken and placed in the refrigerator. The specimen was centrifuged in a subsequent step using a 0.45 μM filter and 10 mL of it for 15 min at 2000 rpm. As a result, A specific quantity of the solution has been diluted with PBS to a pH of 6.0 and put into a 25 mL volumetric flask. Then, different doses of levodopa have been added to these diluted urine samples.

At the hospital at King Khalid University, blood samples were taken from healthy individuals. After that, 0.15 mL of perchloric acid has been mixed with 1 mL of blood that was then mixed for 1 min in a vortex before being centrifuged for 15 min at 2500 rpm. After that, 10 mL of the supernatant was dissolved in PBS (pH = 6.0).

Levodopa tablets, which contain 25.0 mg of the active ingredient each, were analyzed by dissolving the necessary amount in 25 mL of PBS to get an appropriate concentration. To guarantee total disintegration, this combination was subsequently exposed to ultrasonic sonication for 30 min. The solution was filtered after sonication, and the liquid phase was collected in a 100 mL volumetric flask. The resultant samples were diluted with PBS to get the proper concentrations after this filtering procedure was carried out five times. DPV, a voltammetric method, was used for the measurements. An external calibration approach was used for quantification. A SCE was used as the potential range for the DPV measurements, which were performed at a scan rate of 0.05 V/s.

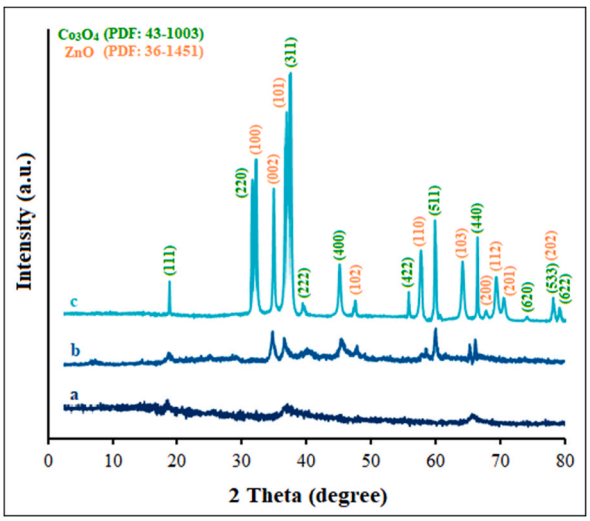

Fig. 1. XRD patterns of ZnO/Co_3O_4 nanocomposite at (a) 0, (b) 200 and (c) 400 W irradiation power.

3. Result and discussion

3.1. ZnO/Co_3O_4 nanocomposite surface characterization

3.1.1. X-ray diffraction

Fig. 1 depicts how the ultrasonic irradiation powers of 0, 200, and 400 W affect the rate of crystallization and the production of particle constituents. At 0, 200, and 400 W of irradiation power, each diffraction peak is flawlessly indexed to the cubic Co_3O_4 structure (PDF#43–1003) and wurtzite ZnO structure (PDF#36–1451) [52]. Fig. 1 (curve a) lack of a peak in the X-ray diffractograms of the sample produced when the ultrasonic irradiation power was absent indicates that either the product's crystallinity has become too low to be detectable or the powder is amorphous. Here, the peak intensities' comparison for ZnO/Co_3O_4 nanocomposite diffraction peaks demonstrates that increasing the sonication output's irradiation power improves the nanocomposite's purity (Fig. 1 (curve b)). This process occurs as a result of the destruction of by-products during the obliteration of ZnO/Co_3O_4 nanocomposite materials using greater ultrasonic irradiation (Fig. 1 (curve c)). This graph shows the impact of varying ultrasonic irradiation strength on the peak ZnO/Co_3O_4 nanocomposite intensity. The specimen with the greatest radiation power hence exhibits higher relative ZnO/Co_3O_4 nanocomposite trait diffraction peak intensities. According to Fig. 1, increasing sonication power results in the formation of smaller

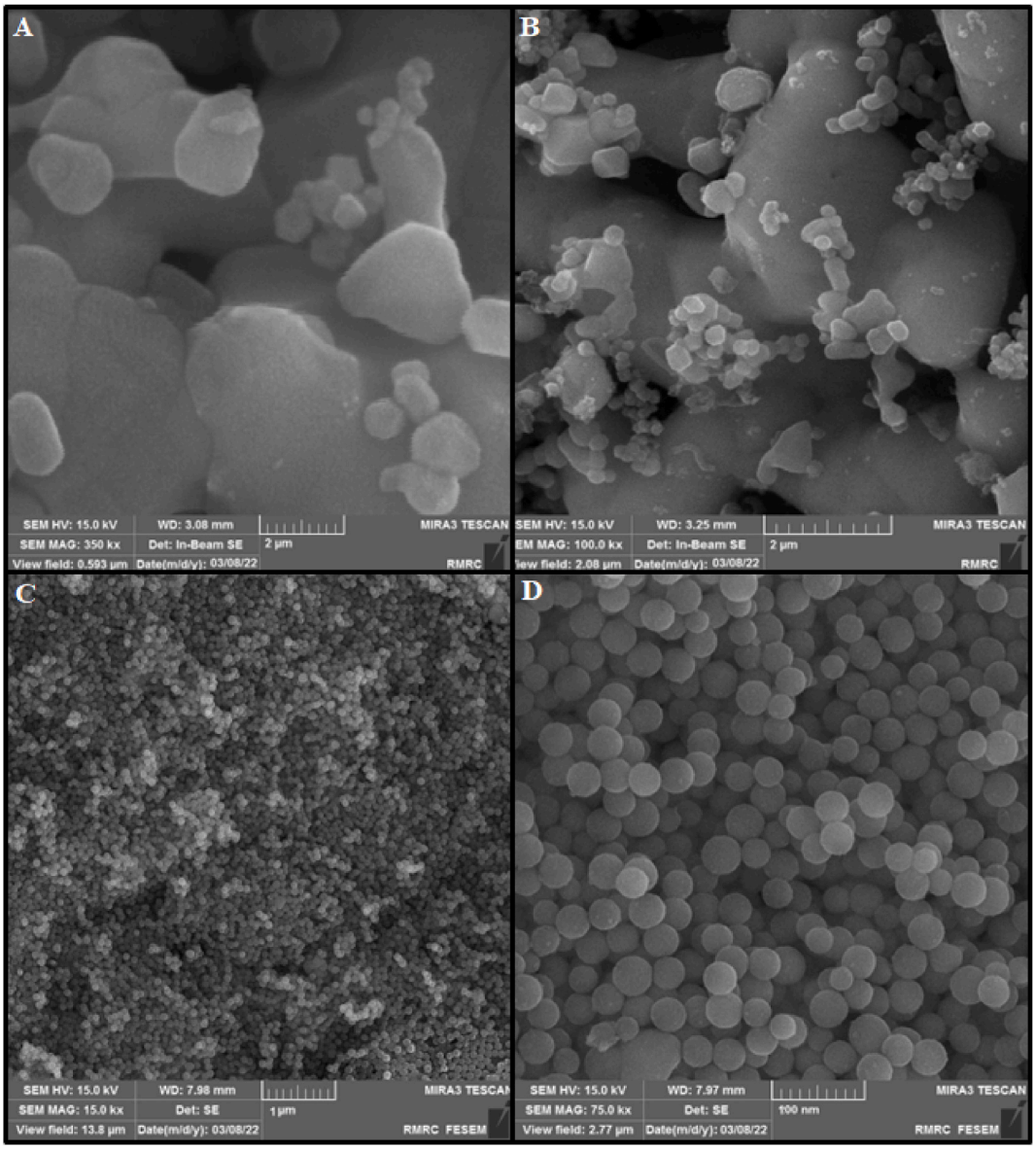

Fig. 2. FESEM images of ZnO/Co_3O_4 nanocomposite at (a) 0, (b) 200, (c) and (d) 400 W irradiation power.

ZnO/Co_3O_4 crystals.

3.1.2. Morphology

Using FESEM evaluation, particles' shape and their dispersion, as well as their size have been evaluated. Fig. 2 shows how the ultrasonic power affects the morphology of the particles. Fig. 2a illustrates that the particles' shape is amorphous when ultrasonic irradiation is absent. Additionally, the particle size has been bigger than the nanoscale size at 200 W of ultrasonic irradiation power (Fig. 2b). However, the ZnO/Co_3O_4 nanocomposite sample exhibits spherical particles at 400 W ultrasonic irradiation power (Fig. 2c). The particle size distribution ranges from 30 nm to 40 nm at 400 W ultrasonic irradiation power, as shown in Fig. 2d (high resolution FESEM image).

By causing bubbles to develop and collapse, ultrasonic irradiation raises the pressure and temperature in the solution. A shift in bubble deterioration symmetry results from the cavitation that happens when solid particles are present in such an event at the particle proximity. Additionally, when cavitation occurs distant from the particles, the bubble collapses, creating a very turbulent flow inside the solution. Consequently, cavitation causes such distinct nanoparticle morphologies to emerge under varied circumstances during ultrasonic irradiation. According to the SEM picture, the amount of particles that accumulate inside the specimen is lessened when ultrasonic irradiation is present. An incidence like this is a sign that nanoparticle dispersion inside this specimen is common and is caused by the formation and collapse of micro-bubbles [53]. Clearly, the length of the ultrasonic irradiation strength correlated with a reduction in particle size (Fig. 2). The rate of particle size reduction after treating specimens with higher ultrasonic power was a higher than it was after treating specimens with lower ultrasonic power.

As shown in Fig. 3, the elemental composition of the ZnO/Co_3O_4 nanocomposite was detected using EDX to assess the material purity. The EDX spectrum of the ZnO/Co_3O_4 nanocomposite clearly shows the presence of oxygen, zinc and cobalt without any contaminants. Fig. 3 displays EDX mapping pictures of ZnO/Co_3O_4 nanocomposite that demonstrate that the generated product is a combination of oxygen, zinc and cobalt.

3.2. Characterization of modified electrode

The ZnO/Co_3O_4 NC/SPE's CV curve in a 0.5 M $[Fe(CN)6]^{3-/4-}$ solution is shown in Fig. 4, with 0.1 M KCl acting as the supporting electrolyte. Fig. 4A illustrates how the effective surface area of the modified and bare electrodes was measured at different scan speeds using the CV technique and a 0.5 mM $[Fe(CN)6]^{3-/4-}$ probe. After that, a reversible process was analyzed using the Randles-Sevcik equation (Eq. 1) in the following way [54]:

$$Ipa = \pm (2.69 \times 10^5)\, n^{3/2}\, A\, D^{1/2}\, C\, \nu^{1/2} \quad (1)$$

Here, n = 1 and D = 7.6×10^{-6} $cm^2\ s^{-1}$ for 0.5 mM $[Fe(CN)_6]^{3-/4-}$ in the 0.1 M KCl electrolyte, respectively, denote the number of transferred electrons, A for the electrode surface area, D for the diffusion coefficient, C for the $[Fe(CN)_6]^{3-/4-}$ concentration (mol cm^{-3}), and ν for the scan rate. For bare SPE and ZnO/Co_3O_4 NC/SPE (Fig. 4B), the true surface area was calculated based on the slope from the

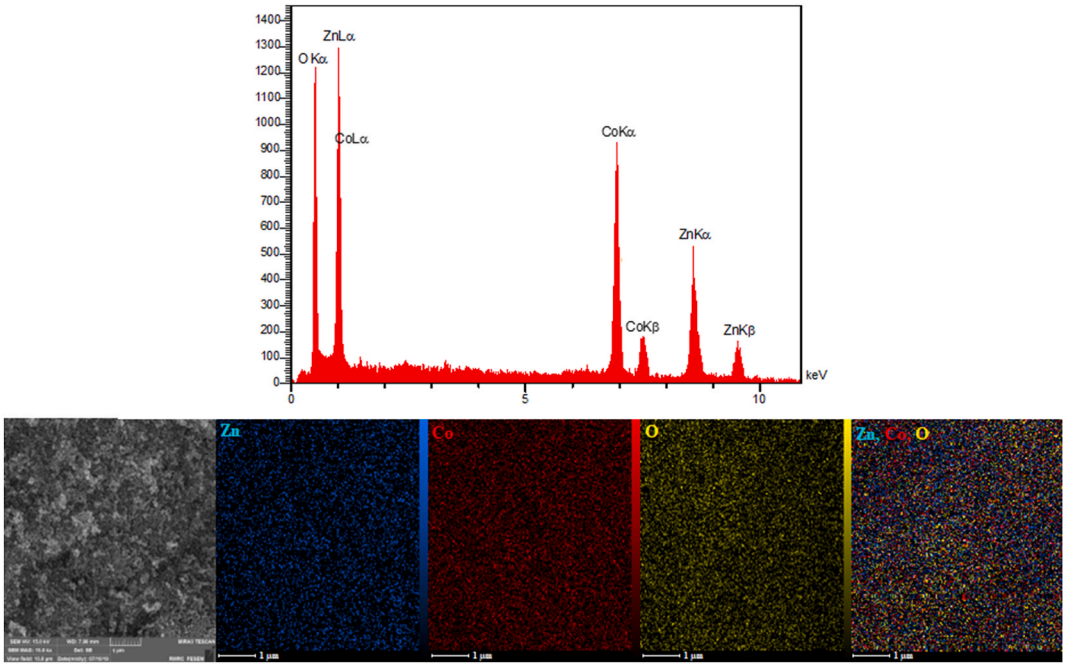

Fig. 3. EDX spectra and elemental mapping of ZnO/Co_3O_4 nanocomposite at 200 W irradiation power.

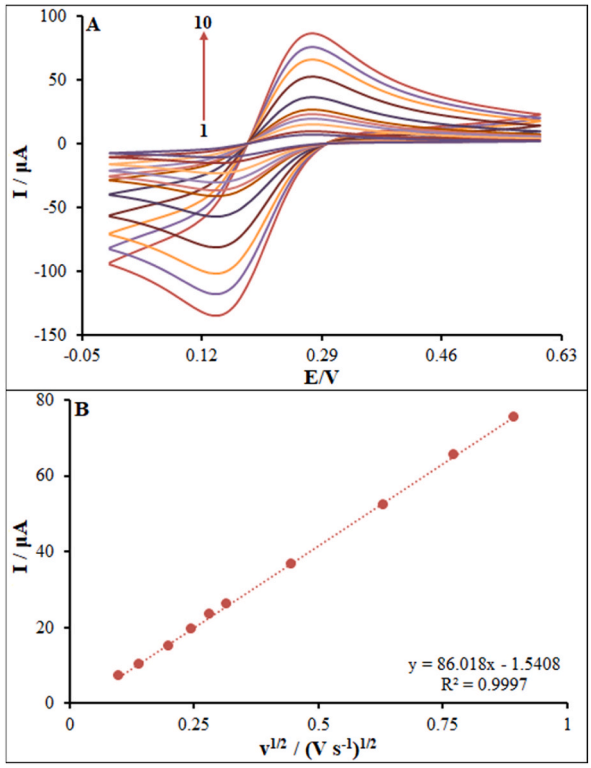

Fig. 4. (A) CVs of ZnO/Co_3O_4 NC/SPE in the presence of 0.5 mM $[Fe(CN)_6]^{3-}$ solution in aqueous 0.1 M KCl at various scan rates (from inner to outer curve): 10, 20, 30, 40, 50, 60, 70, 80, 90, 100, 200, 300, 400, 500, 600, 700 and 800 mV s^{-1}. (B) The plot of peak currents vs. $\upsilon^{1/2}$.

I_{pa}-$\nu^{1/2}$ plot [33,34], which was 0.11 cm^2 and 0.24 cm^2, respectively. Consequently, the ZnO/Co3O4 NC/SPE's surface area was 2.18 times larger than the naked SPE's, in that order. The surface area and electrocatalytic activity of the ZnO/Co_3O_4 nanocomposite on the oxidation process of levodopa at pH 6.0 may be the cause of the higher peak current of analyte oxidation on the ZnO/Co_3O_4 NC/SPE surface.

3.3. Electrochemical behavior of levodopa

At a scan rate of 50 mV s^{-1} in PBS (0.1 M, pH 6.0), CVs were acquired for 95.0 µM levodopa using three distinct electrode setups: bare SPE (curve b), ZnO/Co_3O_4 NC/SPE (curve c), and ZnO/Co_3O_4 NC/SPE without levodopa (curve a) (Fig. 5). Levodopa showed an irreversible, single anodic peak with a peak potential of 510 mV and a peak current of 2.67 µA on the naked SPE surface (curve b). Conversely, the ZnO/Co_3O_4 NC/SPE (curve c) showed the largest anodic peak for levodopa, with a peak current of 14.23 µA and a

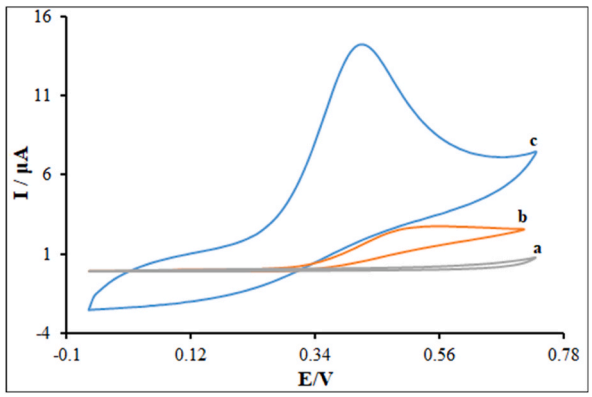

Fig. 5. CVs of a) ZnO/Co_3O_4 NC/SPE in 0.1 M PBS (pH = 6.0), b) bare SPE and c) ZnO/Co_3O_4 NC/SPE in the presence of levodopa (60.0 µM) in PBS at a pH 6.0, respectively. In all cases, the scan rate was 50 mV s^{-1}.

voltage of 425 mV. The ZnO/Co_3O_4 nanocomposite's improved characteristics are responsible for the notable rise in peak current on the ZnO/Co_3O_4 NC/SPE. Levodopa oxidation on the electrode surface is facilitated by the nanocomposite's porous structure, which also boosts electrical conductivity and effective surface area.

3.4. Scan rate and pH

Fig. 6A illustrates the effect of scan rate on the catalytic current of levodopa. Catalytic current (I_{pa}) rose in tandem with the scan rate, which went from 10 to 700 mV s^{-1}. Significantly, the I_{pa} showed a proportionate connection with the scan rate's square root, suggesting an irreversible, diffusion-controlled levodopa oxidation process at the ZnO/Co_3O_4 NC/SPE (Fig. 6A).

The effect of pH on the catalytic current of 100.0 μM levodopa in a phosphate buffer solution was investigated using DPV (Fig. 7). Levodopa's catalytic current increases gradually up to pH 6.0, after which it begins to decline (Fig. 7A). This implies that, in these circumstances, levodopa measurement is best done at a pH of 6.0. Furthermore, Fig. 7B shows that shifting the solution's pH between 3.0 and 7.0 causes the peak potential to move towards less positive values, suggesting that proton transfer plays a role in the electrochemical process. Peak potential (Ep) and solution pH were linearly correlated, and the resulting slope, Ep = −0.0497 pH + 0.47229, is quite similar to the Nernstian value [54]. This result implies that, as shown in Scheme 1, an equal amount of protons and electrons are transported throughout this electrochemical process.

3.5. Chronoamperometry study

Levodopa specimen chronoamperometry was compared to SCE at 475 mV using ZnO/Co_3O_4 NC/SPE. The chronoamperometric results for various specimen concentrations of levodopa in pH 6.0 PBS are displayed in Fig. 8. For the chronoamperometric evaluation of electro-active moieties at transfer restricted state, the Cottrell equation (Eq. 2) is utilized [54]:

$$I = nFAD^{1/2}C_b\pi^{-1/2}t^{-1/2} \quad (2)$$

D and C_b represent the diffusion coefficient ($cm^2\ s^{-1}$) and bulk concentration (mol cm^{-3}), respectively. Using the best fits for various

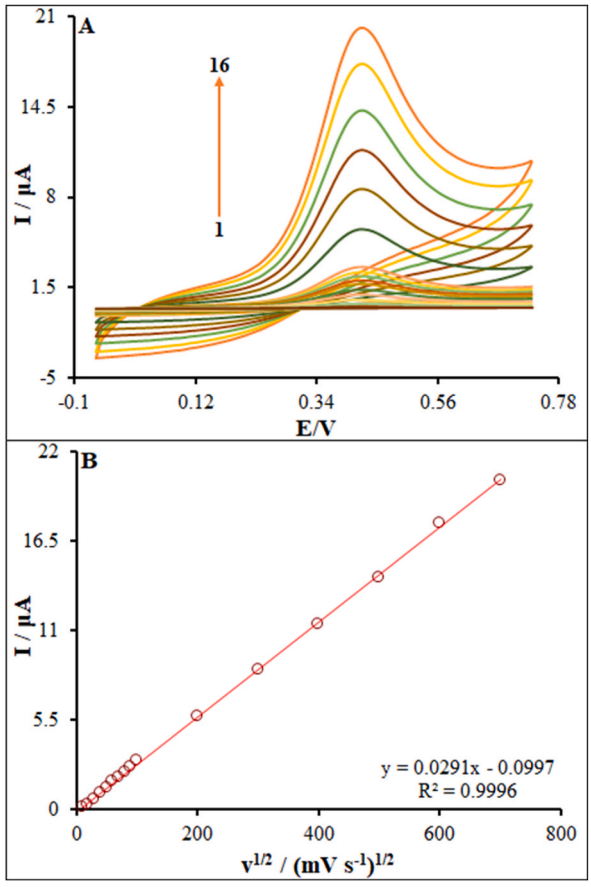

Fig. 6. (A) CVs of ZnO/Co_3O_4 NC/SPE in pH 6.0 in the presence of levodopa (60.0 μM) at various scan rates (from inner to outer curve): 10, 20, 30, 40, 50, 60, 70, 80, 90, 100, 200, 300, 400, 500, 600 and 700 mV s^{-1}. (B) The plots of peak currents vs. $\upsilon^{1/2}$.

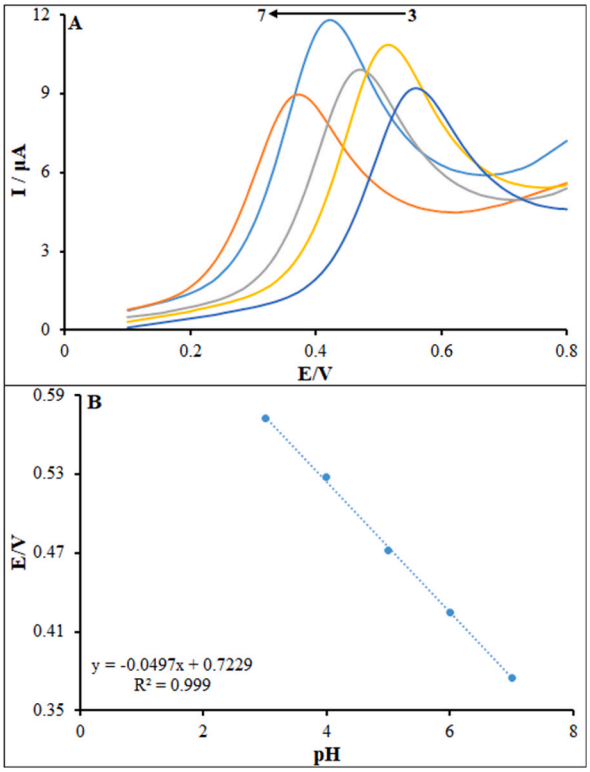

Fig. 7. (A) Effect of pH on the peak currents for the oxidation of levodopa (100.0 µM) pH = 3–7. (B) Plots of peak potential vs. pH. Scan rate: 50 mV s^{-1}.

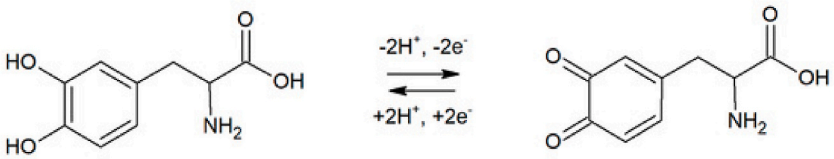

Scheme 1. Probable oxidation mechanism for levodopa [55].

levodopa concentrations, an I vs. $t^{-1/2}$ plot was made based on the empirical data displayed in Fig. 8A. The resulting straight-line slopes were then plotted versus levodopa concentrations in Fig. 8B. The average D value, as derived by the Cottrell equation and the final Fig. 8C plot slope, is 9.76 × 10^{-5} cm^2/s.

3.6. Detection of levodopa

We have measured the levodopa concentration in ZnO/Co_3O_4 NC/SPE using DPV. As the levodopa concentration is changed, Fig. 9A shows the differential pulse voltammetric response at the ZnO/Co_3O_4 NC/SPE. Levodopa calibration plots (Fig. 9B) demonstrate a linear connection in the 0.001–800.0 µM range with a correlation value of 0.9997. Additionally, the detection limit (S/N = 3) was 0.81 nM.

The analytical efficacy of alternative electrochemical methods and the as-fabricated electrode for levodopa was examined (Table 1). Table 1 illustrates how our proposed electrochemical electrode for levodopa sensing fared in comparison to earlier electrochemical methods [55–62], with an improved detection limit and sensitivity. Consequently, the sensor as-fabricated might be able to detect the tiny amounts of the medicine being studied in a range of media. Additionally, a SPE electrode was used in the creation of the sensor since it has several advantages over other electrodes, including as lower background current, greater accessibility, simplicity of customization, and cost.

3.7. Interferences study

The impact of different components on the measurement of levodopa was examined using the mixed solutions approach. When the

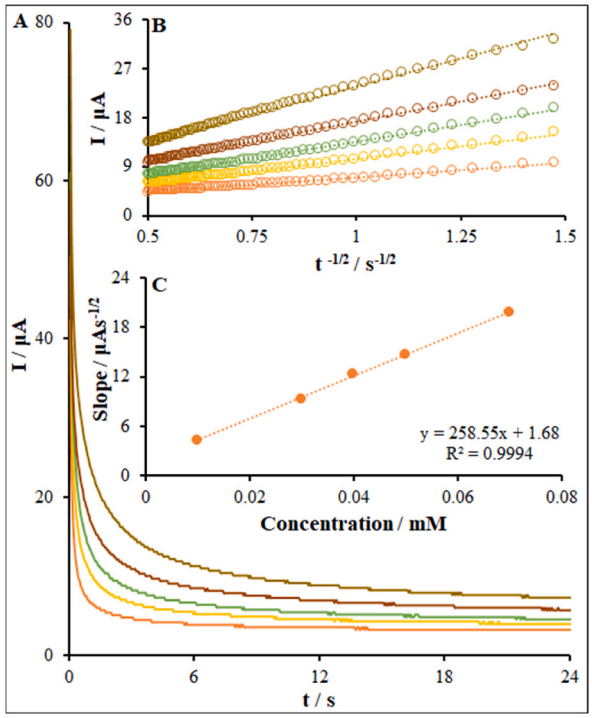

Fig. 8. (A) Chronoamperograms obtained at ZnO/Co_3O_4 NC/SPE in 0.1 M PBS (pH 6.0) for different concentrations of levodopa (from inner to outer curve): 0.01, 0.03, 0.04, 0.05 and 0.07 mM. (B) Plots of I *vs.* $t^{-1/2}$ obtained from chronoamperograms 1–5. (C) Plot of the slope of the straight lines against levodopa concentration.

recommended procedure was applied for the measurement of 50.0 μM levodopa under ideal circumstances (with relative standard deviations of 5 %), no interference was seen when 100-fold cysteine, glutamic acid, aspirin, glucose, tyrosine, K^+, Fe^{2+}, Cu^{2+}, Fe^{3+}, Pb^{2+}, Na^+, Cl^-, and F^- were added.

3.8. Stability and reproducibility

The ZnO/Co_3O_4 NC/SPE stability test was conducted on the sensor for a period of 30 days. The sensor had attained stability, as evidenced by the findings, which revealed that the peak current was maintained at 99.2 % of its initial value (Fig. 10).

Six independently generated ZnO/Co_3O_4 NC/SPE duplicates were used to evaluate the repeatability of the sensor and the dependability of the production process. In 0.1 M PBS (pH 6.0) containing 60.0 μM levodopa, ZnO/Co_3O_4 NC/SPE DPVs were observed; the average currents were 14.25 μA with an RSD of 3.12 %. At the same ZnO/Co_3O_4 NC/SPE surface, repeated studies with 60.0 μM levodopa (n = 15) produced average currents of 14.25 μA with an RSD of 2.98 %. The enhanced level of consistency shown by the altered electrode was demonstrated.

3.9. Detection of levodopa in real samples

To evaluate the viability of the ZnO/Co_3O_4 NC/SPE in the real sample, levodopa was assessed in real samples (levodopa pills, urine samples). Levodopa was not detected in the urine specimens. Levodopa was thus added in a predetermined quantity to the sample solutions. The conventional addition method was used to determine the levodopa dosage. The recoveries for this modified electrode range from 98.0 to 102 %, as Table 2 illustrates. These results imply that levodopa may be detected in real samples using the proposed modified electrode. To evaluate the accuracy and precision of the DPV technique, the high-performance liquid chromatography (HPLC) method [10] was used (Table 2). Statistical analysis show that there is no significant difference in the outputs generated by the two procedures.

4. Conclusion

This study's ZnO/Co_3O_4 nanocomposite was effectively made with the use of ultrasonic technology. Examined was the impact of ultrasonic irradiation power on nanoparticle production and associated properties. By using a ZnO/Co_3O_4 nanocomposite as a modifier in a screen-printed electrode (ZnO/Co_3O_4 NC/SPE), a new sensor was created to measure levodopa. The oxidation peak current of levodopa was significantly increased because of the catalytic activity of ZnO/Co_3O_4 NC due to its elevation of electron transfer rate.

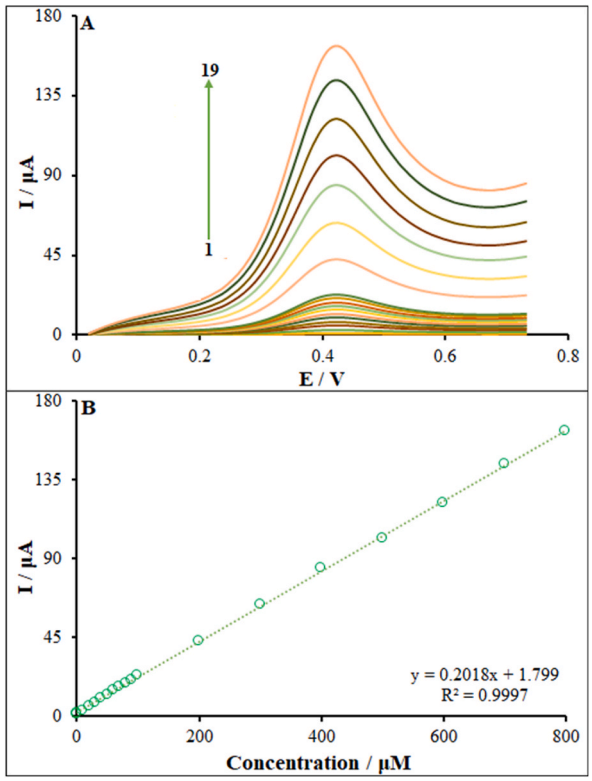

Fig. 9. (A) DPVs of the levodopa at the ZnO/Co_3O_4 NC/SPE in PBS (pH 6.0) at the scan rate of 50 mV s^{-1}, Concentrations from inner to outer of curves: levodopa (0.001, 0.01, 0.1, 1.0, 5.0, 10.0, 20.0, 30.0, 40.0, 50.0, 60.0, 70.0, 80.0, 90.0, 100.0, 200.0, 300.0, 400, 500, 600, 700 and 800.0 (µM). (B) Plots of I vs. Concentrations.

Table 1
Performance comparison of ZnO/Co_3O_4 NC/SPE for the determination of levodopa with other electroanalytical methods.

Method	Modifier	Linear range	Detection limit	Ref.
Voltammetry	Gold nanoparticles supported in activated charcoal with an epichlorohydrin-reticulated chitosan film	50.0 nM-10.0 µM	8.2 nM	[55]
Voltammetry	Hollow-structure porphyrin zirconium-based MOF	0.1–130.0 µM	3.0 nM	[56]
Voltammetry	Carbon nanotube	0.16–2.08 mM	13.87 µM	[57]
Voltammetry	Graphene nanoplatelets and graphitized multi-walled carbon nanotubes with cationic exchange functionalized polymer	0.5–40.0 µM	850.0 nM	[58]
Voltammetry	Multi-walled carbon nanotubes	0.9–85.0 µM	0.38 µM	[59]
Voltammetry	NiO nanoparticle/ionic liquid	0.7–900.0 mM	0.4 µM	[60]
Voltammetry	Nickel hydroxide nanoparticles/multi-walled carbon nanotubes	0.1–300.0 µM	0.075 µM	[61]
Voltammetry	Multiwalled carbon nanotube/chitosan composite	2.0–220.0 µM	0.6 µM	[62]
Voltammetry	NiO/Co_3O_4 nanocomposite	0.001–800.0 µM	0.81 nM	This work

The results demonstrated that levodopa oxidation is catalyzed at pH = 6.0 and that the peak potential of levodopa is lowered by 425 mV to a less positive potential at the modified electrode surface. Notably, our recommended sensor material showed excellent stability, robust anti-interfering activity, and outstanding repeatability. The modified electrode with voltammetric measurement was successfully used to determine levodopa in genuine samples. The electrode is easy to use, but making it demands sophisticated skills.

Ethics statement

We have complied with all relevant ethical regulations. All procedures conform to the principles outlined in the declaration of Helsinki and Ethics committee of King Khalid University (KKU230083) has approved the experiments. All participants were over 18 years of age to donate human samples and all research subjects signed an informed consent form.

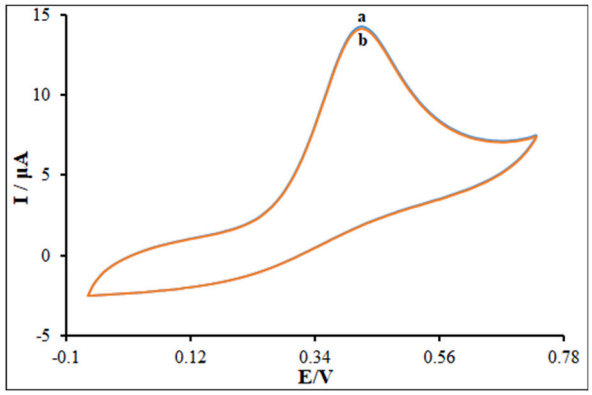

Fig. 10. CVs of modified electrode (a) (containing 60.0 µM of levodopa) and (b) after 30 days.

Table 2
Determination of levodopa in tablet and urine samples using ZnO/Co_3O_4 NC/SPE (n = 5).

Sample	Detected (µM)	Added (µM)	Founded by proposed biosensor (µM)[a,b]	Founded by published method [10] (µM)[a,c]	Recovery (%)[b]	Recovery (%)[c]
Human blood serum	ND[d]	10.0	9.8 ± 0.28	9.9 ± 0.24	98.0	99.0
		15.0	14.9 ± 0.19	15.1 ± 0.25	99.3	100.6
Urine	ND[d]	20.0	20.1 ± 0.29	20.2 ± 0.33	100.5	101.0
		25.0	25.2 ± 0.22	24.8 ± 0.27	100.8	99.2
Levodopa tablet	5.0	10.0	15.3 ± 0.17	15.2 ± 0.21	102.0	101.3
		15.0	19.8 ± 0.16	19.7 ± 0.19	99.0	98.5

[a] Mean ± standard deviation for n = 5.
[b] Proposed method.
[c] Published method [10].
[d] Not detect.

Data availability statement

Data will be made available on request.

CRediT authorship contribution statement

Tan Wanga: Writing – original draft, Formal analysis. **Nadhir N.A. Jafar:** Writing – review & editing, Investigation. **Afrah Majeed Ahmed Al-Rihaymee:** Writing – review & editing, Investigation. **Dheyaa Yahaia Alhameedi:** Data curation. **Fadhil A. Rasen:** Methodology. **Furqan S. Hashim:** Validation. **Talib Kh Hussein:** Writing – original draft. **Montather F. Ramadan:** Visualization. **Kasim Kadhim Alasedi:** Writing – review & editing. **Muath Suliman:** Supervision, Investigation. **Ahmed Hussien Alawadi:** Methodology.

Declaration of competing interest

The authors declare that they have no known competing financial interests or personal relationships that could have appeared to influence the work reported in this paper.

Acknowledgment

The authors express their gratitude to the Deanship of Scientific Research at King Khalid University for funding this work through the Large Research Group Project under grant number RGP.02/375/44.

References

[1] R. Banu, B.E. Kumara Swamy, Poly (Bromocresol purple) incorporated pencil graphite electrode for concurrent determination of serotonin and levodopa in presence of L-Tryptophan: a voltammetric study, Inorg. Chem. Commun. 141 (2022) 109495.
[2] C. Yu, Q. Cao, T. Tu, Y. Cai, L. Fang, X. Ye, B. Liang, Differential coulometry based on dual screen-printed strips for high accuracy levodopa determination towards Parkinson's disease management, J. Pharm. Biomed. Anal. 190 (2020) 113498.
[3] A.L. Sanati, F. Faridbod, M.R. Ganjali, Synergic effect of graphene quantum dots and room temperature ionic liquid for the fabrication of highly sensitive voltammetric sensor for levodopa determination in the presence of serotonin, J. Mol. Liq. 241 (2017) 316–320.

[4] W. Liang, M. Gao, Y. Li, Y. Tong, B.C. Ye, Single-atom electrocatalysts templated by MOF for determination of levodopa, Talanta 225 (2021) 122042.
[5] M. Pourhajghanbar, M. Arvand, M. Farahmand Habibi, Surface imprinting by using bi-functional monomers on spherical template magnetite for selective detection of levodopa in biological fluids, Talanta 254 (2023) 124136.
[6] G. Fabbrini, J.M. Brotchie, F. Grandas, M. Nomoto, C.G. Goetz, Levodopa-induced dyskinesias, Mov. Disord. 22 (2007) 1379–1389.
[7] H.L. Klawans, C. Goetz, D. Bergen, Levodopa-induced myoclonus, Arch. Neurol. 32 (1975) 331–334.
[8] F.K. Goodwin, Psychiatric side effects of levodopa in man, JAMA 218 (1971) 1915–1920.
[9] C. Loutelier-Bourhis, H. Legros, J.J. Bonnet, J. Costentin, C.M. Lange, Gas chromatography/mass spectrometric identification of dopaminergic metabolites in striata of rats treated with L-DOPA, Rapid Commun. Mass Spectrom. 18 (2004) 571–576.
[10] K.V. Özdokur, E. Engin, Ç. Yengin, H. Ertaş, F.N. Ertaş, Determination of Carbidopa, Levodopa, and Droxidopa by high-performance liquid chromatography–tandem mass spectrometry, Anal. Lett. 51 (2018) 73–82.
[11] R.P. Ribeiro, J.C. Gasparetto, R. de Oliveira Vilhena, T.M.G. de Francisco, C.A.F. Martins, M.A. Cardoso, R. Pontarolo, A. Teixeira, K. de Carvalho, Simultaneous determination of levodopa, carbidopa, entacapone, tolcapone, 3-O-methyldopa and dopamine in human plasma by an HPLC–MS/MS method, Bioanalysis 7 (2015) 207–220.
[12] S.M. Alam, M. Mainul Karim, S.H. Lee, S.M. Wabaidur, H.Y. Chung, J.H. Choi, M. Kang, Development of a sensitive flow-injection-chemiluminescence detection method for the determination of levodopa, Luminescence 23 (2008) 327–332.
[13] C. Martinez-Lozano, T. Perez-Ruiz, V. Tomas, O. Val, Determination of epinephrine, norepinephrine, dopamine and l-DOPA in pharmaceuticals by a photokinetic method, Analyst 116 (1991) 857–859.
[14] L. Liu, Y. Zhang, L. Tang, H. Zhong, D. Danzeng, C. Liang, X. Li, The neuroprotective effect of *Byu d mar* 25 in LPS-induced alzheimer's disease mice model, J. Evid. Based Complementary Altern. Med. 2021 (2021) 8879014.
[15] P.S. Ganesh, M. Govindasamy, S.Y. Kim, D.S. Choi, H.U. Ko, R.A. Alshgari, C.H. Huang, Synergetic effects of Mo_2C sphere/SCN nanocatalysts interface for nanomolar detection of uric acid and folic acid in presence of interferences, Ecotoxicol. Environ. Saf. 253 (2023) 114694.
[16] J. Li, J. Luo, L. Liu, H. Fu, L. Tang, The genetic association between apolipoprotein E gene polymorphism and Parkinson disease: a meta-Analysis of 47 studies, Medicine 97 (2018) e12884.
[17] L. Ghasemi, Sh Jahani, M. Ghazizadeh, M.M. Foroughi, Simultaneous determination of amitriptyline and venlafaxine using a novel voltammetric sensor of carbon paste electrode modified with octahedral Pd^{2+}-doped Co_3O_4 composite, Mater. Chem. Phys. 296 (2023) 127176.
[18] W. Zeng, L. Yu, J. Wu, F. Wang, X. Liu, S. Ren, D. Zhang, B. Lian, M. Hu, L. Cao, Clinical characteristics and long-term follow-up outcomes of myelin oligodendrocyte glycoprotein antibody-associated disease in Han Chinese participants, Medicine 102 (2023) e35391.
[19] S.E. Elugoke, O.E. Fayemi, A.S. Adekunle, P.S. Ganesh, S.Y. Kim, E.E. Ebenso, Sensitive and selective neurotransmitter epinephrine detection at a carbon quantum dots/copper oxide nanocomposite, J. Elctroanal. Chem. 929 (2023) 117120.
[20] M. Amare, G. Menkir, Differential pulse voltammetric determination of salbutamol sulfate in syrup pharmaceutical formulation using poly(4-amino-3-hydroxynaphthalene sulfonic acid) modified glassy carbon electrode, Heliyon 3 (2017) e00417.
[21] B.H. Lapizco-Encinas, Y.V. Zhang, P.P. Gqamana, J. Lavicka, F. Foret, Capillary electrophoresis as a sample separation step to mass spectrometry analysis: a primer, TrAC Trends Anal. Chem. 164 (2023) 117096.
[22] M.M. Foroughi, Sh Jahani, S. Rashidi, Simultaneous detection of ascorbic acid, dopamine, acetaminophen and tryptophan using a screen-printed electrode modified with woolen ball-shaped La^{3+}/TiO_2 nanostructure as a quadruplet nanosensor, Microchem. J. 198 (2024) 110156.
[23] C. Yeh, C. Zhang, W. Shi, M. Lo, G. Tinkhauser, A. Oswal, Cross-frequency coupling and intelligent neuromodulation, Cyborg Bionic Syst. 4 (2023) 34.
[24] M. Akilarasan, E. Tamilalagan, S.M. Chen, S. Maheshwaran, C.H. Fan, M.A. Habila, M. Sillanpää, Rational synthesis of rare-earth lanthanum molybdate covered reduced graphene oxide nanocomposites for the voltammetric detection of Moxifloxacin hydrochloride, Bioelectrochemistry 146 (2022) 108166.
[25] Q. Wan, X. Wu, Z. Hou, Y. Ma, L. Wang, Organophotoelectrocatalytic $C(sp^2)$–H alkylation of heteroarenes with unactivated $C(sp^3)$–H compounds, Chem. Commun. 60 (2024) 5502–5505.
[26] B.T. Djonse Justin, N. Blaise, H. Gomdje Valery, Investigation of the photoactivation effect of TiO_2 onto carbon-clay paste electrode by cyclic voltammetry analysis, Heliyon 9 (2023) e13474.
[27] J. Wang, Z. Xi, B. Niu, R. Gao, Z. Xu, Catalytic pyrolysis of waste-printed circuit boards using a Cu/Fe bimetal synergistic effect to enhance debromination, Sustainability 16 (2024) 3009.
[28] T. Iranmanesh, Sh Jahani, M.M. Foroughi, M. Shahidi Zandi, H. Hasani Nadiki, Synthesis of La_2O_3/MWCNT nanocomposite as the sensing element for electrochemical determination of theophylline, Anal. Methods 12 (2020) 4319–4326.
[29] Q.Q. Shen, X.H. Jv, X.Z. Ma, C. Li, L. Liu, W.T. Jia, L. Qu, L.L. Chen, J.X. Xie, Cell senescence induced by toxic interaction between α-synuclein and iron precedes nigral dopaminergic neuron loss in a mouse model of Parkinson's disease, Acta Pharmacol. Sin. 45 (2024) 268–281.
[30] K. Phasuksom, N. Ariyasajjamongkol, A. Sirivat, Screen-printed electrode designed with MXene/doped-polyindole and MWCNT/doped-polyindole for chronoamperometric enzymatic glucose sensor, Heliyon 10 (2024) e24346.
[31] X. Cao, X. Cao, H. Guo, T. Li, Y. Jie, N. Wang, Z.L. Wang, Piezotronic effect enhanced label-free detection of DNA using a Schottky-contacted ZnO nanowire biosensor, ACS Nano 10 (2016) 8038–8044.
[32] S. Park, S. Kim, G.-J. Sun, D.B. Byeon, S.K. Hyun, W.I. Lee, C. Lee, ZnO-core/ZnSeshell nanowire UV photodetector, J. Alloy Compd. 658 (2016) 459–464 658.
[33] J. Yang, S. Tang, W. Mei, Y. Chen, W. Yi, P. Lv, G. Yang, Valorising lignocellulosic biomass to high-performance electrocatalysts via anaerobic digestion pretreatment, Biochar 6 (2024) 23.
[34] H. Colak, E. Karakose, Tm-doped ZnO nanorods as a TCO for PV applications, J. Rare Earths 36 (2018) 1067–1073.
[35] J. Wang, X. Jiang, L. Zhao, S. Zuo, X. Chen, L. Zhang, Z. Lin, X. Zhao, Y. Qin, X. Zhou, X.Y. Yu, Lineage reprogramming of fibroblasts into induced cardiac progenitor cells by CRISPR/Cas9-based transcriptional activators, Acta Pharm. Sin. B 10 (2020) 313–326.
[36] S. Park, Enhancement of hydrogen sensing response of ZnO nanowires for the decoration of WO_3 nanoparticles, Mater. Lett. 234 (2019) 315–318.
[37] S. Sun, M. Wang, X. Chang, Y. Jiang, D. Zhang, D. Wang, Y. Zhang, Y. Lei, $W_{18}O_{49}/Ti_3C_2T_x$ Mxene nanocomposites for highly sensitive acetone gas sensor with low detection limit, Sens. Actuators, B 304 (2020) 127274.
[38] H. Zhang, Q. Zou, Y. Ju, C. Song, D. Chen, Distance-based support vector machine to predict DNA N_6-methyladine modification, Curr. Bioinform 17 (2022) 473–482.
[39] J.Y. Park, H.-Y. Kim, D. Rana, D. Jamal, A. Katosh, Surface area controlled synthesis of porous TiO_2 thin films for gas sensing applications, Nanotechnology 28 (2017) 095502.
[40] C. Cao, J. Wang, D. Kwok, Z. Zhang, F. Cui, D. Zhao, M.J. Li, Q. Zou, webTWAS: a resource for disease candidate susceptibility genes identified by transcriptome-wide association study, Nucleic Acids Res. 50 (2022) D1123–D1130.
[41] Z. Cai, S. Park, Enhancement mechanisms of ethanol-sensing properties based on Cr_2O_3 nanoparticle-anchored SnO_2 nanowires, J. Mater. Res. Technol. 9 (2020) 271–281.
[42] S. Liu, H. Wang, Y. Liu, N. Xu, X. Zhao, Sliding-mode surface-based adaptive optimal nonzero-sum games for saturated nonlinear multi-player systems with identifier-critic networks, Neurocomputing 584 (2024) 127575.
[43] S. Huang, G. Zong, N. Xu, H. Wang, X. Zhao, Adaptive dynamic surface control of MIMO nonlinear systems: a hybrid event triggering mechanism, Int. J. Adapt. Control Signal Process. 38 (2024) 437–454.
[44] J. Wang, S. Fan, Y. Xia, C. Yang, S. Komarneni, Room-temperature gas sensors based on ZnO nanorod/Au hybrids: visible-light-modulated dual selectivity to NO_2 and NH_3, J. Hazard Mater. 381 (2020) 120919.
[45] X.P. Lei, Z. Li, Y.H. Zhong, S.P. Li, J.C. Chen, Y.Y. Ke, A. Lv, L.J. Huang, Q.R. Pan, L.X. Zhao, X.Y. Yang, Z.S. Chen, Q.D. Deng, X.Y. Yu, Gli 1 promotes epithelial-mesenchymal transition and metastasis of non-small cell lung carcinoma by regulating snail transcriptional activity and stability, Acta Pharm. Sin. B 12 (2022) 3877–3890.

[46] J. Lee, S.H. Lee, S.Y. Bak, S.Y. Kim, Y. Kim, K. Woo, S. Lee, Y. Lim, M. Yi, Improved sensitivity of α-Fe_2O_3 nanoparticle-decorated ZnO nanowire gas sensor for CO, Sensors 19 (2019) 1903.
[47] L. Zhang, S. Deng, Y. Zhang, Q. Peng, H. Li, P. Wang, X. Fu, X. Lei, A. Qin, X.Y. Yu, Homotypic targeting delivery of siRNA with artificial cancer cells, Adv. Healthc. Mater. 9 (2020) e1900772.
[48] A. Aziz, N. Tiwale, A.S. Hodge, J.S. Attwood, G. Divitini, E.M. Welland, Core-shell electrospun polycrystalline ZnO nanofibers for ultra-sensitive NO_2 gas sensing, ACS Appl. Mater. Interfaces 10 (2018) 43817–43823.
[49] J. Chen, X. Yan, W. Liu, Q. Xue, The ethanol sensing property of magnetron sputtered ZnO thin films modified by Ag ion implantation, Sens. Actuators, B 160 (2011) 1499–1503.
[50] T. Zhou, T. Zhang, J. Deng, R. Zhang, Z. Lou, L. Wang, P-type Co_3O_4 nanomaterials based gas sensor: preparation and acetone sensing performance, Sens. Actuators, B 242 (2017) 369–377.
[51] S.K. Min, H. Kim, Y. Noh, K.S. Choi, S.P. Chang, Fabrication of highly sensitive and selective acetone sensor using (p)-Co_3O_4 nanoparticle-decorated (n)-ZnO nanowires, Thin Solid Films 714 (2020) 138249.
[52] L. Zhang, X. Jiang, J. Liu, J. Wang, Y. Sun, Facile synthesis of mesoporous ZnO/Co_3O_4 microspheres with enhanced gas-sensing for ethanol, Sens. Actuators, B 221 (2015) 1492–1498.
[53] R. Torkzadeh-Mahani, M.M. Foroughi, Sh Jahani, M. Kazemipour, H. Hassani Nadiki, The effect of ultrasonic irradiation on the morphology of NiO/Co_3O_4 nanocomposite and its application to the simultaneous electrochemical determination of droxidopa and carbidopa, Ultrason. Sonochem. 56 (2019) 183–192.
[54] A.J. Bard, L.R. Faulkner, Electrochemical Methods: Fundamentals and Applications, second ed., Wiley, New York, 2001.
[55] A.M. Santos, A. Wong, L.M.C. Ferreira, F.L.F. Soares, O. Fatibello-Filho, F.C. Moraes, F.C. Vicentini, Multivariate optimization of a novel electrode film architecture containing gold nanoparticle-decorated activated charcoal for voltammetric determination of levodopa levels in pre-therapeutic phase of Parkinson's disease, Electrochim. Acta 390 (2021) 138851.
[56] L. Liu, F. Li, T. Liu, S. Chen, M. Zhang, Porphyrin zirconium-based MOF dispersed single Pt atom for electrocatalytic sensing levodopa, J. Electroanal. Chem. 921 (2022) 116701.
[57] L. Fang, Y. Zhang, Y. Liu, J. Shou, H. Liu, L. Li, Flexible electrochemical sensor for simultaneous determination of levodopa and uric acid based on carbon nanotube fibers, Microchem. J. 199 (2024) 110101.
[58] B. Nigović, New approach on sensitive analysis of pimavanserin, levodopa and entacapone based on synergistic effect of graphene nanoplatelets and graphitized carbon nanotubes in functionalized polymer matrix, Elctrochim Acta 439 (2023) 141700.
[59] J.B. Raoof, R. Ojani, M. Amiri-Aref, M. Baghayeri, Electrodeposition of quercetin at a multi-walled carbon nanotubes modified glassy carbon electrode as a novel and efficient voltammetric sensor for simultaneous determination of levodopa, uric acid and tyramine, Sens. Actuators, B 166 (2012) 508–518.
[60] M. Fouladgar, H. Karimi-Maleh, V. Kumar-Gupta, Highly sensitive voltammetric sensor based on NiO nanoparticle room temperature ionic liquid modified carbon paste electrode for levodopa analysis, J. Mol. Liq. 208 (2015) 78–83.
[61] A. Babaei, M. Sohrabi, A.R. Taheri, Highly sensitive simultaneous determination of L-dopa and paracetamol using a glassy carbon electrode modified with a composite of nickel hydroxide nanoparticles/multi-walled carbon nanotubes, J. Electroanal. Chem. 698 (2013) 45–51.
[62] A. Babaei, M. Babazadeh, A selective simultaneous determination of levodopa and serotonin using a glassy carbon electrode modified with multi-walled carbon nanotube/Chitosan composite, Electroanalysis 23 (2011) 1726–1735.